

DSN Microwave Antenna Holography

D. J. Rochblatt

B. L. Seidel

Radio Frequency and Microwave Subsystems Section

The DSN microwave antenna holography project will obtain three-dimensional "pictures" of the large DSN antenna surfaces. These "pictures" must be of sufficient resolution to allow adjustment of the reflector panels to an rms surface of 0.5 mm (0.25 mm, goal).

This article outlines the major parameters and equations needed to define a holographic measurement system and then discusses the proof of concept demonstration measurement that was made at DSS-43 (Australia) that resulted in contour maps with spatial resolution of 7 m in the aperture plane and resolution orthogonal to the aperture plane of 0.7 mm.

I. Introduction

Microwave holography as applied to antennas is a technique that utilizes the Fourier transform relationship between the complex far-field radiation pattern of an antenna and the complex aperture field distribution. Contour maps of a reflector antenna surface can be inferred from the phase portion of the aperture field distribution. This technique has now been successfully applied to a number of large reflector antennas around the world.

To be useful, the map must have sufficient resolution to allow the individual panels of a reflector antenna to be adjusted to an accuracy that will allow the antenna to operate at high efficiency.

Presently, optical techniques are used to measure the large DSN tracking antennas. This technique requires removal of

major components of the antenna system (because of blockage) and requires up to 8 weeks of antenna down time. By contrast, the microwave holography technique leaves the antenna system intact and is estimated to require about 12 hours (of antenna time) to collect the data needed for the requisite resolution on a 64-m antenna. The antenna can then be immediately placed back in operation and the panels can be adjusted over many weeks during normal maintenance periods, a major advantage.

Early attempts at JPL to produce holographic surface maps of a large antenna were conducted using a radio star (3C273) as a far field source. These experiments were conducted using DSS-43 as the test antenna and DSS-42 as the reference antenna. Both the VLBI and the connected element interferometer (CEI) equipments were used to take data. These data, while providing the basis for our first low resolution holographic surface maps, also pointed out unanticipated structural

dynamics problems and the futility of using radio stars for an illumination source.

II. Antenna Efficiency

The ultimate performance of a large, steerable, reflector antenna is limited by imperfections of the reflecting surface. The size of the panels that form the surface of the antenna and the allowed level of losses due to surface inaccuracies dictate the required resolution of the measurements. From the size of the panels on the DSN antennas, we determine that a spatial resolution of 0.4 m is needed in the x, y (aperture) plane. For a maximum of 0.1 dB degradation in antenna efficiency due to surface imperfections, the rms surface error (ϵ) must be no greater than 0.012λ (where λ is the wavelength):

$$\epsilon_{-0.1 \text{ dB}} \leq 0.012 \lambda \quad (1)$$

The relationship between the efficiency of a physical antenna and a hypothetical antenna with absence of phase errors across its surface is given (for $\epsilon/\lambda \leq 1/4\pi$) by (Refs. 1, 2, 3)

$$\frac{\eta_A}{\eta_0} = \exp - \left(\frac{4\pi\epsilon}{\lambda} \right)^2 + \left(\frac{2r_c}{D} \right) \left[1 - \exp - \left(\frac{4\pi\epsilon}{\lambda} \right)^2 \right] \quad (2)$$

where

- η_A = antenna aperture efficiency
- η_0 = antenna aperture efficiency with zero phase error
- ϵ = rms surface deviation
- λ = wavelength
- r_c = correlation radius
- D = antenna diameter

For totally random surface phase errors, $r_c = 0$, Eq. (2) reduces to its first term. When r_c is significant relative to D , the second term in Eq. (2) adds to the first term to yield a higher efficiency than the case where the errors are indeed totally random.

Therefore, in a worst case, we see that

$$\frac{\eta_A}{\eta_0} = \exp - \left(\frac{4\pi\epsilon}{\lambda} \right)^2 \quad (3)$$

In general, the rms surface error (ϵ) of a perfectly focused DSN antenna at an elevation angle of 45 deg is composed of the following three major components (Ref. 4):

- (1) surface panel setting errors (SPS)
- (2) primary surface panel manufacturing errors (PSP)
- (3) subreflector manufacturing errors (SM)

Presently, these components for the DSN 64-m antennas are

$$\text{SPS} = 0.48 \text{ mm}$$

$$\text{PSP} = 0.89 \text{ mm}$$

$$\text{SM} = 0.30 \text{ mm}$$

for a total rms surface error of $\epsilon = 1.06$ mm. At an operating frequency of 8440 MHz this rms surface error corresponds to 0.6 dB degradation in antenna efficiency relative to an antenna with a perfect surface. Part of the 64-m antenna upgrade project has set the following goals for improvement in the antenna surface:

$$\text{SPS} = 0.25 \text{ mm}$$

$$\text{PSP} = 0.25 \text{ mm}$$

$$\text{SM} = 0.25 \text{ mm}$$

These goals would result in a total rms surface error at an elevation angle of 45 deg of $\epsilon = 0.44$ mm. At an operating frequency of 8440 MHz, this rms surface error corresponds to 0.1 dB degradation in antenna efficiency relative to an antenna with a perfect surface. This would provide a significant 0.5 dB efficiency improvement from present capability.

III. Spatial Resolution

The first step in the process of acquiring the contour maps is to obtain the antenna complex far field pattern. To do this, two antennas are used connected to a two channel receiver-correlator (Fig. 1) to observe the incoming signal from a far field source. While the (usually smaller) reference antenna is observing the incoming signal on boresight, the test antenna is scanning the transmitting source. Samples of the signal are taken at prescribed points on a (usually convenient) rectangular grid matrix. The number of data points collected is related to the required spatial resolution in the aperture plane. The separation between each data point must be less than one beamwidth.

Consider a square grid containing N^2 sampled data points separated by less than λ/D or one beamwidth (along the scan axis). Let

$$\Delta = \frac{K\lambda}{D} \quad (4)$$

where

Δ = separation between two adjacent sampled data points

λ = wavelength

D = antenna diameter

K = a constant $0.5 < K < 1.0$

The length of each side of the grid is $(N - 1) K(\lambda/D)$ which for large N becomes

$$L = NK \left(\frac{\lambda}{D} \right) \quad (5)$$

where

L = Length of square grid

N^2 = Total number of sampled data points

Consider the Fourier transform of a rectangular pulse extending from $(+N/2)K(\lambda/D)$ to $(-N/2)K(\lambda/D)$ (Fig. 2).

The function transforms from a pulse in the θ domain to a

$$\frac{\sin \left(\frac{\pi NK \lambda x}{D} \right)}{\left(\frac{\pi NK \lambda x}{D} \right)}$$

function in the X domain whose first two nulls occur at $\pm D/K\lambda N$ for a full null width of $2D/K\lambda N$.

We define spatial resolution to be at the 50% width (eliminating the λ) to obtain

$$\delta = \frac{D}{KN} \quad (6)$$

where

δ = spatial resolution in the aperture plane

For a rectangular grid matrix of $N \times N$ data points, N is given by

$$N = \frac{D}{K\delta} \quad (7)$$

For the large DSN antennas where $D = 64$ m and the required spatial resolution based on individual panel size consideration is $\delta = 0.4$ m, and we use $K = 0.8$, the number of sampled data points required is

$$N^2 = \left[\frac{D}{K\delta} \right]^2 = \left[\frac{64}{(0.8)(0.4)} \right]^2 = 40,000$$

or a grid of 200×200 .

Because of symmetry requirements about the boresight, the linear dimension of the required grid must have an odd number of data points. We therefore increase the size of the required grid to 201×201 data points.

IV. Signal-to-Noise Ratio Requirement

It can be shown (L. E. Young, private communication) that the voltage signal-to-noise ratio (SNR) on the aperture (which is related to the surface accuracy) is related to the SNR of a complex correlation taken with both antennas receiving the signal on boresight by

$$\text{SNR}(A) = \frac{\text{SNR}(O)}{N} \quad (8)$$

where

$\text{SNR}(A)$ = signal-to-noise ratio on the aperture

$\text{SNR}(O)$ = signal-to-noise ratio of a complex correlation taken at boresight

N = the square root of the total number of sampled data points (Eq. 7)

Equation (8) is based on the Fourier transform relationship between the complex correlation of a sample in the antenna far field distribution and the complex aperture distribution elements. It is derived using basic error analysis and assuming that each complex element in the aperture distribution has the same error for each sampled data point.

The equivalent accuracy on the aperture is given by

$$\epsilon(a) = \frac{\lambda}{2\pi \text{SNR}(A)} \quad (9)$$

We can now relate the distortion on the surface $\epsilon(s)$ to a distortion on the aperture by (Ref. 5)

$$\epsilon(s) = \frac{\epsilon(a)}{2 \cos \left(\frac{\psi}{2} \right)} \quad (10)$$

where

ψ = Angle between horn to subreflector to main reflector point of distortion.

For the DSN 64-m antenna the angle ψ has a maximum value of about 60 deg where $\epsilon(s)$ assumes the largest value or worst case; hence,

$$\epsilon \equiv \epsilon(s)_{\max} = \frac{\epsilon(a)}{1.73} \quad (11)$$

Using Eqs. (8), (9), (10), and (11), we calculate for SNR(O):

$$\text{SNR} \equiv \text{SNR}(O) = \frac{0.29 N\lambda}{\pi\epsilon} \quad (12)$$

Equation (12) relates the SNR requirement to the rms surface resolution and the number of sampled data points needed. We may use Eq. (7) to express the required voltage SNR as:

$$\text{SNR} = \frac{0.29 D\lambda}{\pi K\delta\epsilon} \quad (13)$$

V. Far-Field Source

The large sampled data array that must be measured in order to obtain a spatial resolution of 0.4 m and the antenna scan rate (the array size needed of 201×201 is independent of the frequency selected for the measurement; see Eq. 7) dictates the time required for the measurement. Because of the antenna mechanical dynamics characteristics, 20 s were needed to move the DSS-43 antenna between adjacent data points. This time is needed for the antenna movement to damp out, if the antenna is to be stopped at each sampled data point. From the above we conclude that more than 200 h would be needed for the measurement alone (independent of frequency), an unacceptable situation. The conclusion that sampled data must be taken while the antenna is continuously scanning is therefore adopted.

Strong artificial sources are needed to provide the required SNR in the short integration times necessitated by continuous scanning.

By allocation, no geosynchronous satellites are permitted in the DSN portion of X-band (8.4 - 8.5 GHz). Geosynchronous satellites are available, Defense Satellite Communications Systems (DSCS II), with transmitting sources at S-band (2.2 GHz). With some modification, the DSN antennas can be fitted to receive the DSCS II signals transmitted at 7.7 GHz.

To achieve the required rms surface precision of 0.5 mm and spatial resolution of 0.4 m in the holography maps, the following SNRs are needed (Eqs. 12, 13): 63.2 dB at 7.7 GHz or 74.0 dB at 2.2 GHz. To achieve the above SNR require-

ments, a geosynchronous satellite with an approximate effective isotropic radiated power (EIRP) of +40 dBm is needed in the direction of the DSN 64-m ground antenna.

VI. Elevation Angle Effects

The N th sampled data points are taken off the M th side lobe given by

$$M = \frac{D}{2\delta} \quad (14)$$

where

M = the outermost side lobe off boresight

For the 64-m DSN antenna,

$$M = 80$$

The elevation angle excursion can now be calculated by

$$\theta_{\max} = M \left(\frac{\lambda}{D} \right) \frac{180}{\pi} \text{ deg}$$

For the 64-m antennas this yields

$$\theta_{2.2 \text{ GHz}} = \pm 9.7 \text{ deg}$$

$$\theta_{7.7 \text{ GHz}} = \pm 2.8 \text{ deg}$$

The wide elevation angle excursions needed for high resolution holography mapping will, to a first order, not smear the "longwave"¹ gravitational distortions of the large reflector. This can be understood in a few different ways. Recall the Fourier transform relationship between the antenna aperture response and its far field response and for a moment observe the relationship:

$$\cos(\omega_0 t) \leftarrow \text{F.T.} \rightarrow \pi [\delta(\omega - \omega_0) + \delta(\omega + \omega_0)]$$

where here

δ = Dirac delta function

The higher the frequency in the time domain, the further apart the delta functions in the frequency domain separate from the $\omega = 0$ axis, and vice versa.

¹We use the term "longwave" to signify large portions of the diameter, say $D/4$ or larger.

This relationship is analogous to the ripple on the antenna surface (the cosine function) which transforms into delta type functions in the antenna far-field pattern. It is clear that long gravitational distortions (low frequency) will reveal themselves in the first few side lobes of the antenna far-field pattern (delta functions close to main axis) while the short-wave ripples (high frequency) will reveal themselves as delta functions in the far side lobes.

The “forgiving” nature of the large antenna holography business is this: in fact, imbedded in the central “core” array (say, 11×11) is the information needed to “see” the long-wave distortions, and this can be obtained with narrower elevation angle excursions. The short time required to scan 11×11 also minimizes possible thermal effects. Imbedded in the “outer limits” of a big array (say, 201×201) is the information needed to see the shortwave “ripples” and these (to a first order) do not depend on elevation angle (these originated at the “factory” and are not due to gravity changes with elevation angle). Thus, we are not much concerned with ± 2.8 deg (X-band) or even ± 9.7 deg (S-band) elevation angle excursions possibly “smearing” the “pictures.”

VII. Data Taking

To enable the completion of a test in a reasonable time (a period of 12 h seems sensible), data must be collected while the antenna is continuously moving. The following analysis is aimed at finding relationships between dynamic range, quantizer resolution, integration time, and scan speed. The latter is limited for the large DSN antennas to a range of 0.001 to 0.25 deg/s (JPL Document 810-5, Rev. D, Volume 1, “Deep Space Network/Flight Project Interface Design Handbook”).

Studying CCIR (Comite Consultatif International Radio) generalized pattern and calculated radiation pattern envelopes for $D/\lambda = 500$ (Ref. 6) reveals that the 80th side lobe may be at -70 dB to -80 dB level relative to the peak of the main lobe.

The first few side lobes of the far-field amplitude pattern for a circular aperture uniformly illuminated antenna can be approximated by

$$h(\theta) = 2 \left[\frac{J_1(\theta)}{\theta} \right] \quad (15)$$

where

$J_1(\theta)$ = Bessel function of the first kind

The rate of change of the pattern with respect to θ is

$$\frac{dh(\theta)}{d\theta} = 2\theta \left[\frac{J_0(\theta) - 2J_1(\theta)/\theta}{\theta^2} \right] \quad (16)$$

where

$$\frac{dJ_1(\theta)}{d\theta} = J_0 - J_1(\theta)/\theta \quad (17)$$

At the first null of $J_1(\theta)$ the slope is

$$\left| \frac{dh(\theta)}{d\theta} \right|_{J_1(\theta) = 0} = \left| 2 \left[\frac{J_0(3.83171)}{3.83171} \right] \right| = 0.2102 \text{ v/rad} \quad (18)$$

where the first zero occurs at $\theta = 3.83171$. This null occurs at a different angle for different antennas and is a function of both λ and D . In our case, it occurs at $1.22 \lambda/D$ off boresight. We can now calculate the change in voltage amplitude ΔV occurring during a small scan $\Delta\theta$ and constrain it to be smaller than one part in 2^{B-1} in its limiting case (where B is the quantizer resolution).

$$\Delta V = \Delta\theta \left[\left| \frac{dh(\theta)}{d\theta} \right|_{J_1(\theta) = 0} \right] \left[\frac{3.83171}{1.22 \frac{\lambda}{D}} \right] \leq \frac{1}{2^{B-1}} \quad (19)$$

A 12-bit signed quantizer is needed for a voltage dynamic range of 66 dB. Using $D = 64$ m, we obtain

$$\text{at S-band:} \quad \Delta\theta_s = 9.03 \times 10^{-5} \text{ deg}$$

$$\text{and at X-band:} \quad \Delta\theta_x = 2.58 \times 10^{-5} \text{ deg}$$

The DSN 64-m antennas have a maximum scan rate of 0.25 deg/s. Let us consider the scan rates in the range of

$$0.010 \text{ deg/s} \leq t_{\text{scan}} \leq 0.25 \text{ deg/s}$$

The integration time is given by

$$\tau = \frac{\Delta\theta}{t_{\text{scan}}} \quad (20)$$

which from Eq. (19) and the scan ranges shown becomes,

$$\text{for S-band:} \quad 9.0 \text{ ms} \geq \tau \geq 0.36 \text{ ms}$$

$$\text{for X-band:} \quad 2.6 \text{ ms} \geq \tau \geq 0.1 \text{ ms}$$

We can estimate the total required measurement time, T , by dividing the scan angle by the scan rate and multiplying by the number of scan lines, adding the retrace time to that number (calculated at the maximum scan rate), and adding 20% for calibration points and antenna mechanical effects:

$$T = N \left[\frac{2\theta}{t_{\text{scan}}} + \frac{2\theta}{0.25} \right] (1.2) \text{ s}$$

We have previously found that the scan angles required are ± 9.7 deg at S-band and ± 2.8 deg at X-band.

The scan rates given earlier, therefore, lead to estimated measurement times, T , of

$$135 \text{ h} \geq T_{\text{S-band}} \geq 10.4 \text{ h}$$

or

$$39 \text{ h} \geq T_{\text{X-band}} \geq 3 \text{ h}$$

Clearly, the higher scan rates are desirable.

Indeed, the final integration time and scan rate selected will depend on the signal source strength, antenna system temperature, bandwidth used, and antenna diameter.

VIII. DSS-43-42 Experiment

Preliminary holographic measurements were conducted at DSS-43-42 using the Tidbinbilla connected element interferometer (C.E.I.). DSS-43, the 64-m antenna, was measured while DSS-42, the 34-m antenna, was used as the reference; 3C273 was used as the signal source at 2.28 GHz with flux density of approximately 35 Jy². The system temperature at zenith is approximately 20 K. The test was done at approximately 40° elevation where the system temperature was ~25 K. The C.E.I. has a detection sensitivity of 50 mJy in 1 s. The IF bandwidth was 12 MHz. The baseline between the two antennas is 194.6 m (1485λ, north-south) and is located near Canberra (Lat. 35.4° S, Long. 149° E). A phase-coherent local-oscillator distribution system is used to make the differential phase insensitive to variation in cable lengths (Ref. 7).

For a given source flux density, the source temperature at the antenna is given by (Ref. 8)

$$T_a = \frac{10^{-26} \eta}{2k} A_g S \quad (21)$$

²Jy = 10⁻²⁶ W/m² Hz

where

T_a = Source temperature at the antenna (K)

η = Antenna efficiency

A_g = Projected geometrical area of the antenna

k = Boltzmann's constant (1.38×10^{-23} J/K)

S = Source flux density (Jy)

1/2 = A factor to account for randomly polarized source

We can now define a minimum detectable signal:

$$\Delta T = \frac{T_s}{[2 B \tau]^{1/2}} \quad (22)$$

where

ΔT = Minimum detectable signal

B = Predetection bandwidth

τ = Postdetection integration time

T_s = System temperature

For the C.E.I., A_g is the geometric mean of the areas of the test and reference antennas:

$$A_g = \pi \left[\frac{D_1 D_2}{4} \right] \quad (23)$$

where

D_1 = Test antenna diameter

D_2 = Reference antenna diameter

Similarly,

$$T_s = \left[T_{s_1} T_{s_2} \right]^{1/2} \quad (24)$$

where

T_s = system temperature

T_{s_1} = Test antenna temperature

T_{s_2} = Reference antenna temperature

We can now define signal to noise ratio of the system as

$$\text{SNR} = \frac{T_a}{\Delta T} \quad (25)$$

Combining Eqs. (21), (22), (23), (24), and (25) yields:

$$\text{SNR} = 4.03 \times 10^{-4} \eta \text{SCD}_1 D_2 \left[\frac{B\tau}{T_{s_1} T_{s_2}} \right]^{1/2} \quad (26)$$

where η is the antenna efficiency and C is the correlation efficiency.

During this experiment an integration time of 10 s was used at each observed point, η is approximately 0.6, and the correlation efficiency is approximately 0.5. This yields

$$\text{SNR} = 72 \text{ dB}$$

A sampling factor $K = 0.8$ was used during the measurement of the 11-X-11 grid, to achieve a spatial resolution of (Eq. 6)

$$\delta = \frac{D}{KN} = \frac{64}{(0.8)(11)} \cong 7 \text{ m}$$

Using Eq. (12), we may calculate ϵ to be equal to 0.03 mm. The hologram presented (Fig. 3) has an rms surface error of 0.7 mm; however, it seems to be well above the noise level.

The data was collected using HA/DEC coordinates, and 20 s were allowed for movement between adjacent sampled points, and 30 s were allowed to move to the boresight for calibration. At each sampled data point, the system was sampled for 10 s (integration time). The data collected during this test were recorded on diskette and brought to JPL for software processing. This software package that produced the plots and maps shown (Figs. 5 through 11) is described in the next section (software development) (Rahmat-Samii, Y., private communication).

In a time difference of approximately 1.5 h, a second C.E.I. measurement was conducted in the exact manner as the first experiment. A presentation of the plots is shown (Fig. 4) which compares well with plots obtained during the first experiment in both amplitude and surface profile contour. The only major difference between the maps is an axial rotation of about 17.5° which results from the change in the source location during the time period between the two experiments (Rahmat-Samii, Y., private communication).

Another set of data was collected at DSS-43-42 using the VLBI block zero system. Using a bandwidth of 1.8 MHz and sampling rate of 3×10^6 samples/s, a voltage SNR of 65 dB was achieved with 10-s integration time.

$$\text{SNR} = CA [B\tau]^{1/2} \quad (27)$$

where

CA = Correlation amplitude on boresight

B = Samples/s

τ = Integration time

$$\text{SNR} = 0.35 [3 \times 10^6 \times 10]^{1/2} \cong 1900$$

The VLBI method proved to be inadequate for the holographic measurements. It doesn't provide any verification of test results on site and the probability of recording "bad" data on tapes and hence not utilizing the time spent for the test in the most efficient way is high. The C.E.I. system provided a SNR 7 dB larger than that obtained from the VLBI system. The data collected using the VLBI technique was therefore never actually processed.

IX. Software Development

The software package that was used is composed of the following parts:

- (1) Residual phase extractor. Strips the residual phase from the original data set (Figs. 5 and 6) which have nominal reference points imbedded (these reference points are measured when both test and reference antennas observe the incoming signal on boresight).

The nominal reference points are considered to be coordinates of some polynomial function (to obtain Fig. 7, second order degree polynomial was used). In the same manner, the program will optimally normalize the amplitude data set to a polynomial function (Fig. 8).

For both the amplitude and phase functions, the Chebychev polynomial may be used to yield better curve fits at the expense of hand checking the result to insure that the function doesn't drop below zero within the domain of normalized points.

- (2) Plotting program. This program generated the plots and maps as shown (Figs. 5 through 11).

- (3) Spiral to columnar transformation program. This program takes data arranged as a spiral configuration (this is the way data was collected thus far using the C.E.I. and VLBI experiment as DSS-43-42. This method of collecting the data will be different in the final system capable of producing high resolution maps), and transform it into a two-dimensional complex array (two values are read for each element).
- (4) Far-field pattern program. This program generates the far-field amplitude and phase from the measured data.
- (5) FFT program. This program computes the inverse fast Fourier transform of the far-field pattern with surface errors. A novel iteration procedure is used to improve the final solution (Ref. 5).

X. Summary

The microwave holography technique has now been successfully used to make surface maps of many of the world's large antennas. The technique allows measurement of the surface with the antenna in an operational configuration. This is contrasted to the traditional optical and/or mechanical methods that often require removal of significant portions of the antenna structure (such as cassegrain feedcone). An optical measurement and panel setting exercise on a DSN 64-m

antenna typically requires that the antenna be taken out of service for about 8 weeks. When operational, microwave holography will require on the order of 12 hours of dedicated test time to collect the data for the surface map. Panel setting can then be performed during normal maintenance periods; a significant improvement in the utilization of a valuable resource.

Holography also allows for inspection of the antenna surface on a routine basis, an option that is not readily available using present optical techniques.

Early microwave holography at JPL was conducted using a natural radio source (3C273). This work pointed out the need to use artificial radio sources (geostationary satellites) in order to obtain the high SNRs needed for short integration times. Additionally, mechanical oscillations in the antenna structure at DSS-43 required us to allow 20 seconds to move the antenna from point to point in the data grid so that the antenna again became stable enough to take data. This will be avoided in the future by continuous scanning across strong artificial sources that require short integration times.

The work performed to date has demonstrated the ability of this technique to produce low-resolution surface maps of the large DSN antennas. Much remains to be done before high resolution surface maps become a reality.

Acknowledgements

The authors wish to thank many people who contributed to this work. Many helpful technical discussions were held with Dan Bathker and Larry Young. We would also like to thank Sam Gulkis, Mike Batty, Dave Jauncey and Bill Peters for supplying and operating the Connected Element Interferometer that was used to obtain the data for this experiment. Special thanks go to Yahya Rahmat-Samii for the software development and data reduction that provided many of the figures in this report.

References

1. Ruze, J., "Antenna Tolerance Theory—A Review," *Proc. IEEE* 54, 1966.
2. Vu, T. B., "Influence of Correlation Intervals and Illumination Taper in Antenna Tolerance Theory," *Proc. IEE* 116, London, 1969.
3. Baars, J. W. M., *IEEE Trans Antennas Propagation AP-21*, 1973.
4. Bathker, D. A., *Radio Frequency Performance of a 210-ft Ground Antenna, X-Band*. JPL Technical Report 32-1417, Jet Propulsion Laboratory, Pasadena, CA, Dec. 15, 1969.
5. Rahmat-Samii, Y., *Surface Diagnosis of Large Reflector Antennas Using Microwave Holography Metrology – An Iterative Approach*, 1983-URSI Symposium on Electromagnetic Theory, Santiago de Compostela, Spain, August 23-26, 1983.
6. Bathker, D. A., *Microwave Performance Characterization of Large Space Antennas*. JPL Publication 77-21, Jet Propulsion Laboratory, Pasadena, CA, May 15, 1977, pp. 4-22.
7. Gulkis, S., Batty, M. J., Jauncey, D. L., and Rayner, P. T., "Tidbinbilla Two-Element Interferometer," *The Astronomical Journal*, Volume 87, No. 6, June 1982.
8. Kraus, J. D., *Radio Astronomy*, McGraw-Hill, 1966.

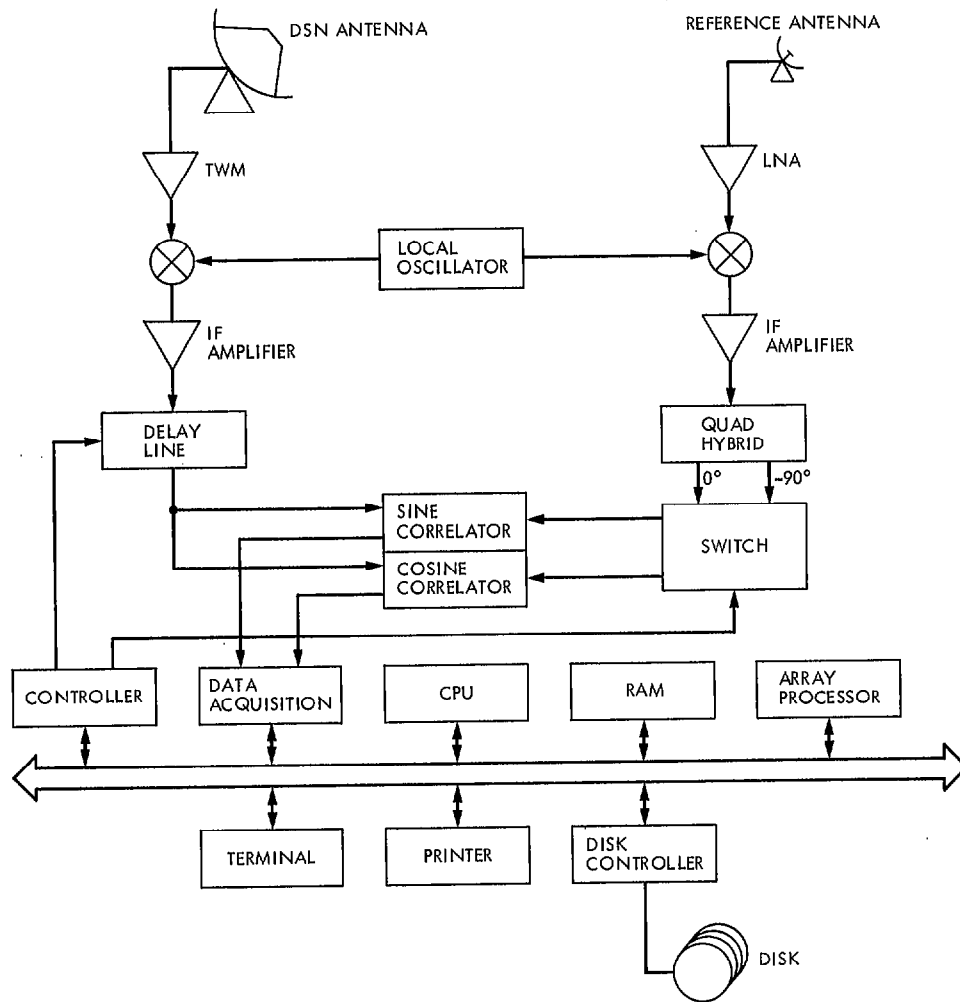


Fig. 1. Holographic mapping receiving system

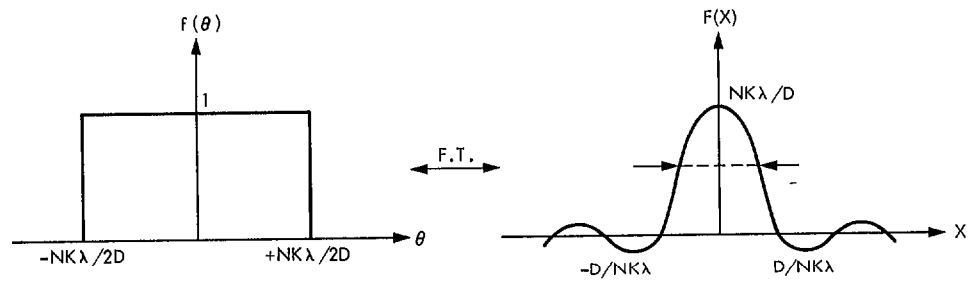


Fig. 2. Fourier transform relationship

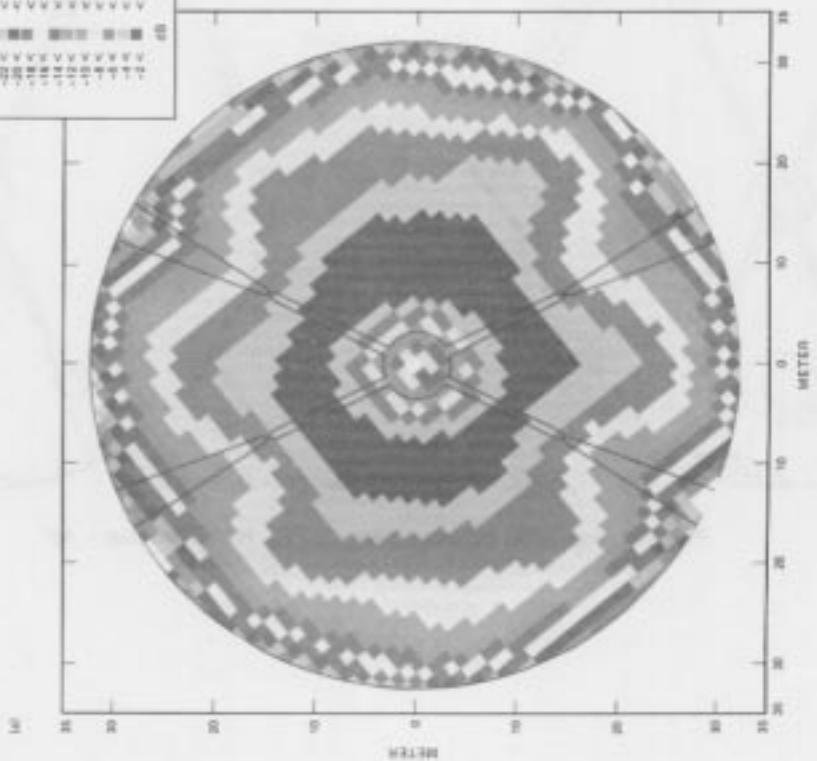
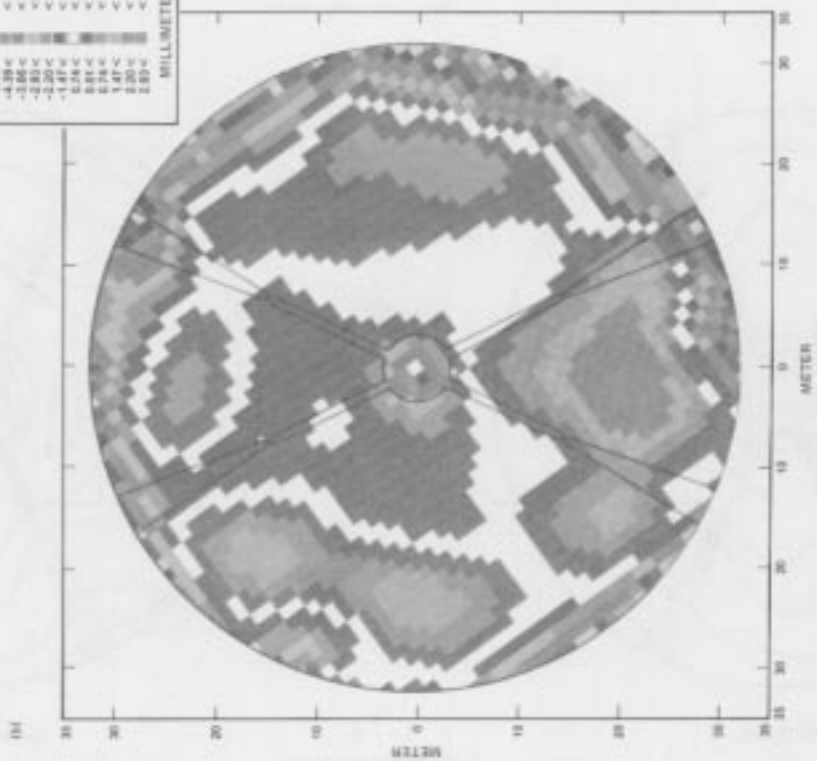
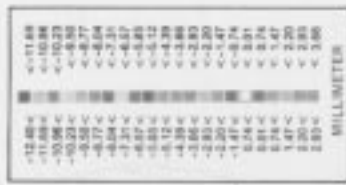


Fig. 3. Gray-level holographic maps of DSS-43: (a) amplitude profile of Tidbinbilla 64-m antenna measured at S-band; (b) surface profile of Tidbinbilla 64-m antenna measured at S-band.

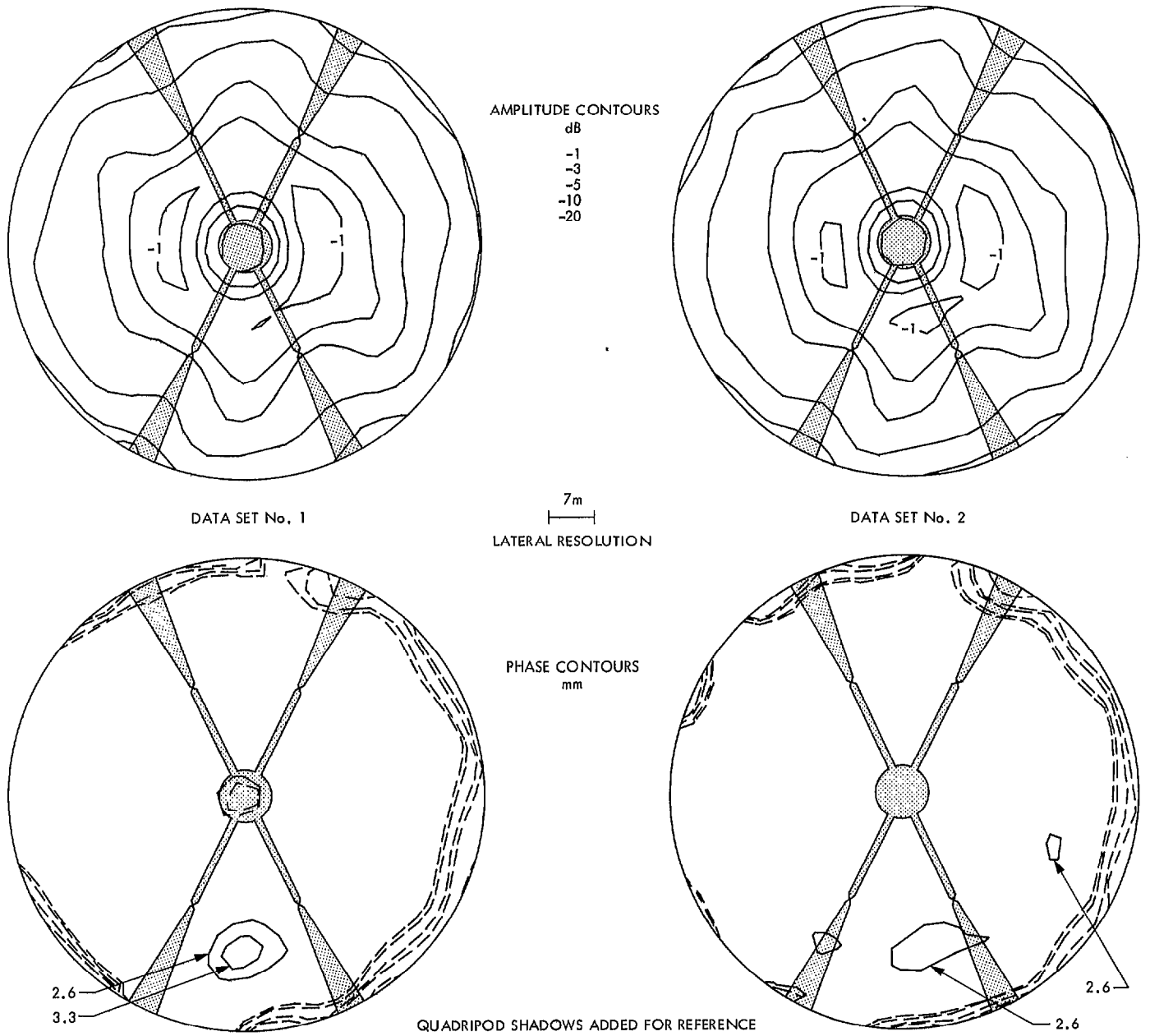


Fig. 4. Holographic surfaces, DSS-43, Feb. 1983, elevation ~ 40°

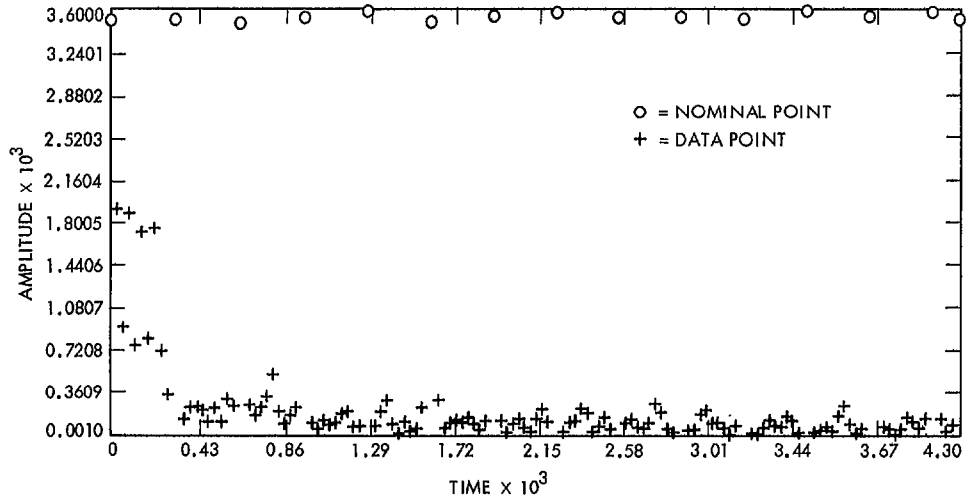


Fig. 5. Measured far-field amplitude data

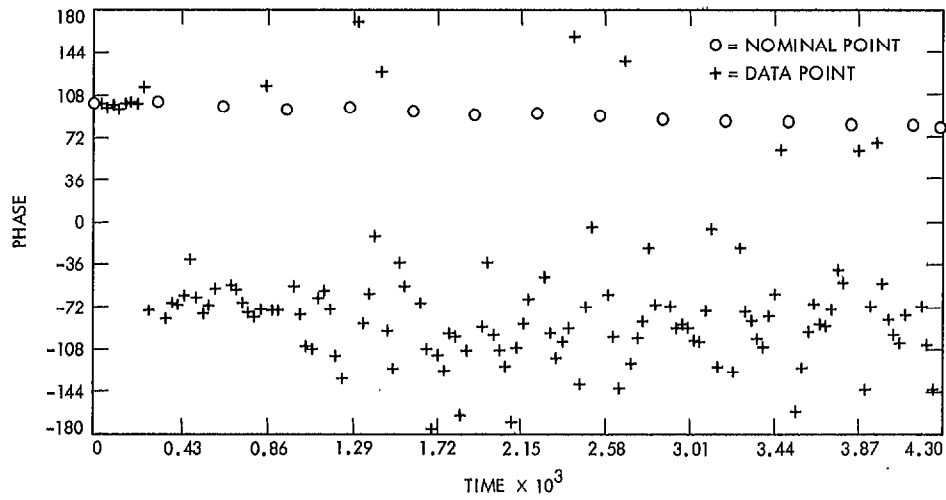


Fig. 6. Measured far-field phase data

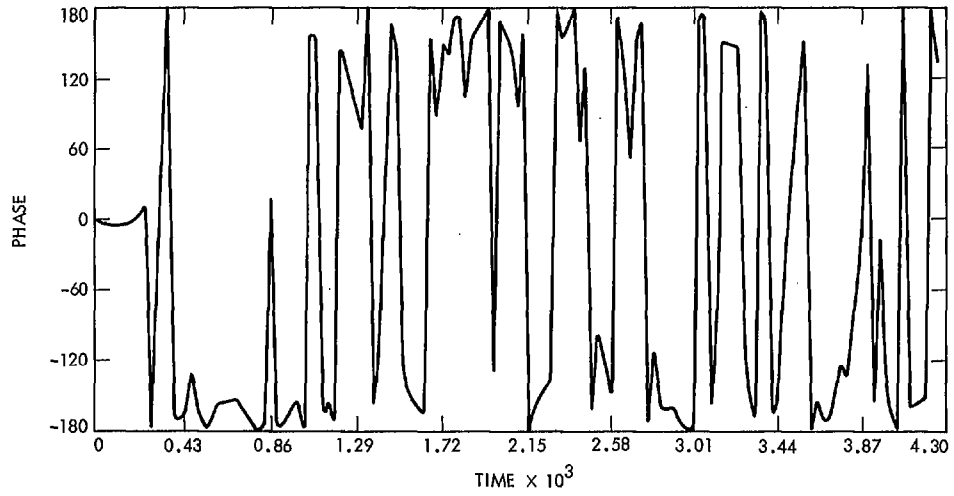


Fig. 7. Adjusted far-field phase data. Residual phase reduced to the range (-180, 180) vs. time.

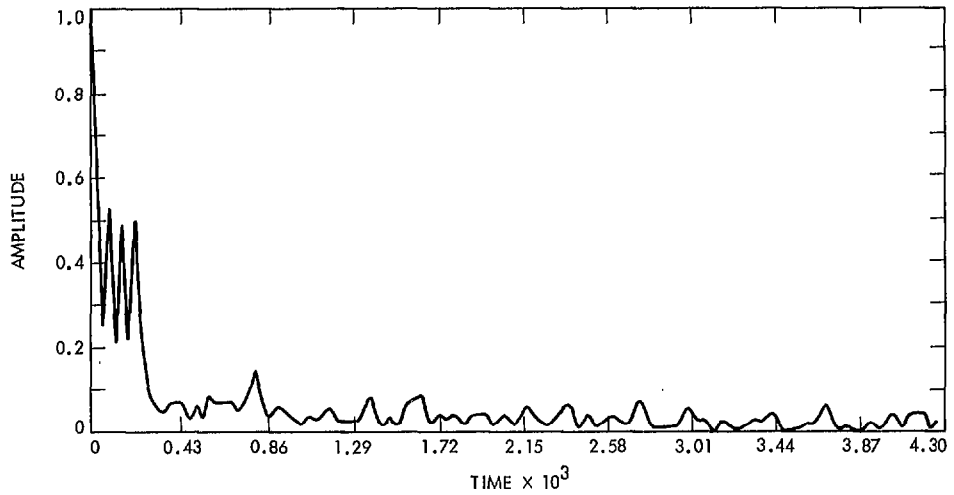


Fig. 8. Adjusted far-field amplitude data. Amplitude normalized to drift curve vs. time.

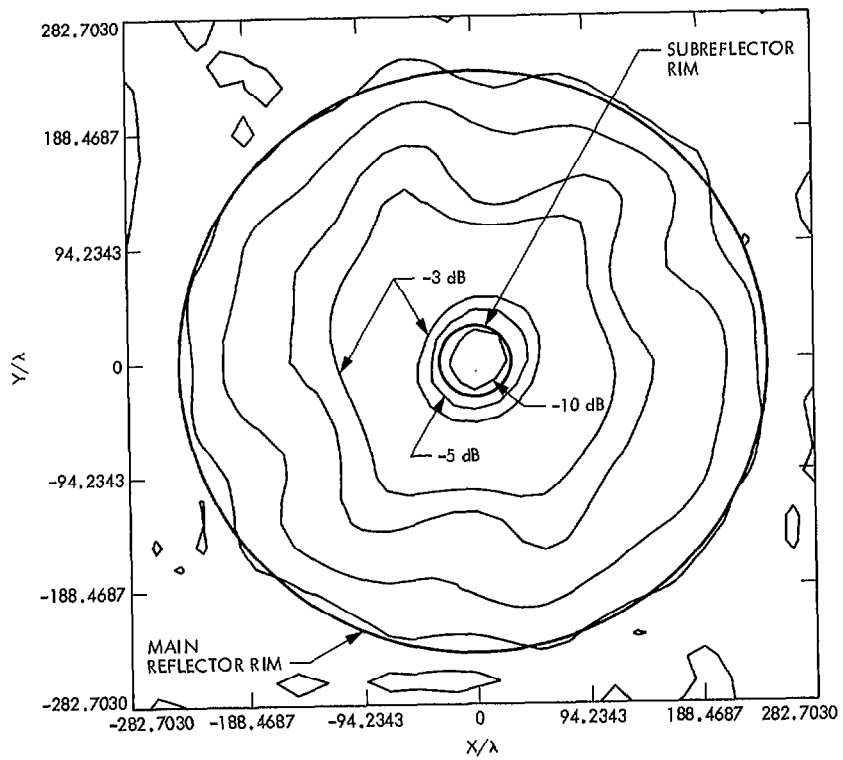


Fig. 9. Contour plot of the reflector aperture amplitude distribution

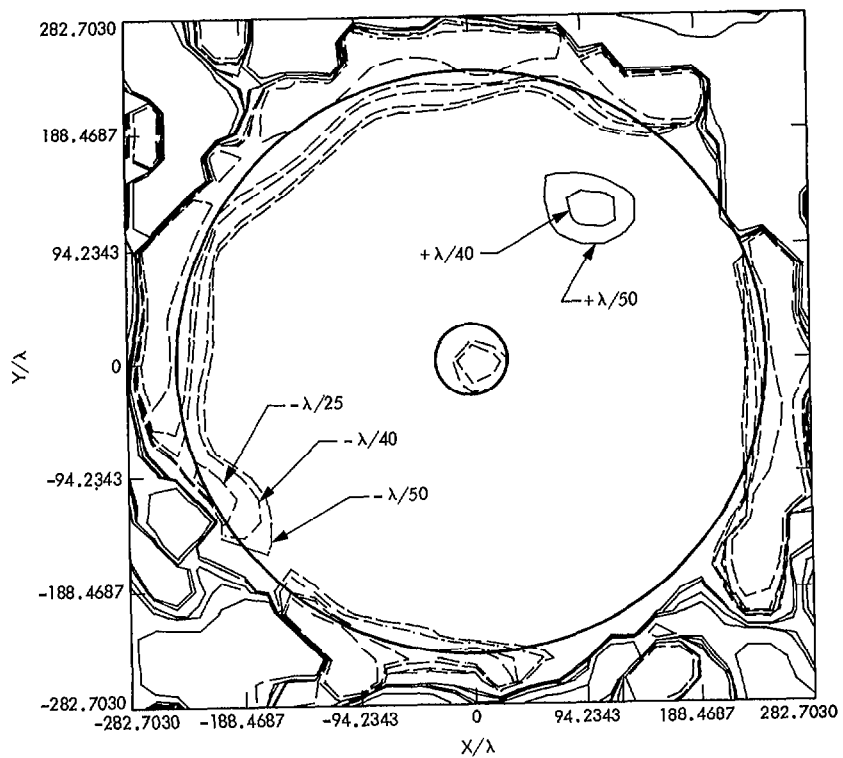


Fig. 10. Contour plot of the surface distortion profile

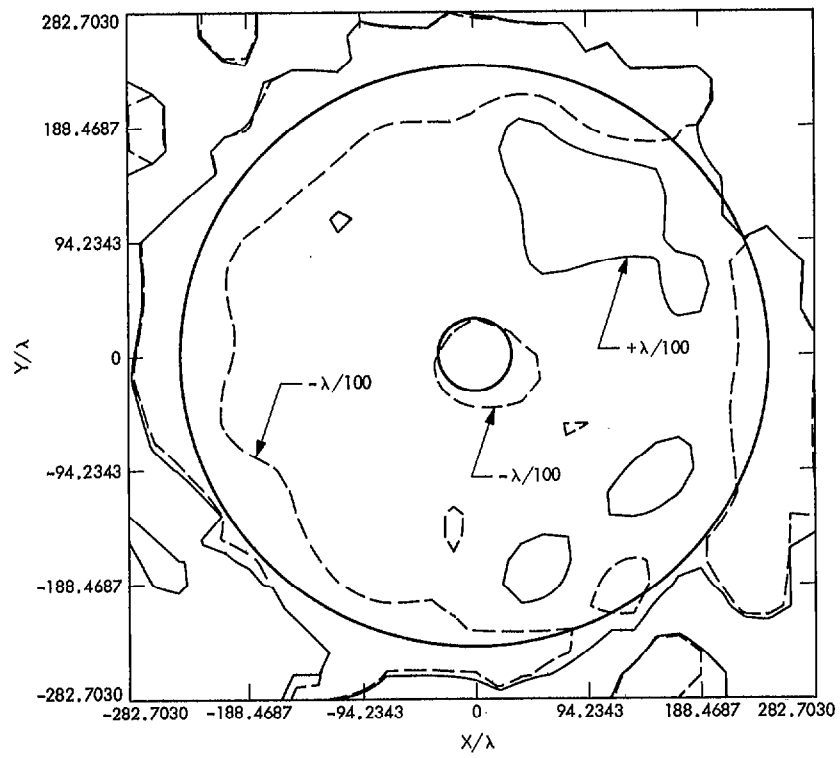


Fig. 11. Contour plot of the surface distortion profile. Contour line is at $\pm 0.01\lambda$.